

Josephson Oscillation and Transition to Self-Trapping for Bose-Einstein-Condensates in a Triple-Well Trap

Bin Liu^{1,2}, LiBin Fu², ShiPing Yang¹, and Jie Liu²

1. College of Physics and Information Engineering,
Hebei Normal University, 050016 Shijiazhuang, China

2. Institute of Applied Physics and Computational Mathematics, P.O. Box 8009 (28), 100088 Beijing, China

We investigate the tunnelling dynamics of Bose-Einstein-Condensates (BECs) in a symmetric as well as in a tilted triple-well trap within the framework of mean-field treatment. The eigenenergies as the functions of the zero-point energy difference between the tilted wells show a striking entangled star structure when the atomic interaction is large. We then achieve insight into the oscillation solutions around the corresponding eigenstates and observe several new types of Josephson oscillations. With increasing the atomic interaction, the Josephson-type oscillation is blocked and the self-trapping solution emerges. The condensates are self-trapped either in one well or in two wells but no scaling-law is observed near transition points. In particular, we find that the transition from the Josephson-type oscillation to the self-trapping is accompanied with some irregular regime where tunnelling dynamics is dominated by chaos. The above analysis is facilitated with the help of the Poincaré section method that visualizes the motions of BECs in a reduced phase plane.

PACS numbers: 03.75.Kk, 03.75.Lm

I. INTRODUCTION

Since the first realization of dilute degenerate atomic gases in 1995, a new epoch for studying the dynamical property of Bose-Einstein Condensates (BECs) comes [1]. For the dilute degenerate gases, essential dynamical property is included in the Gross-Pitaevskii equation (GPE) [2]. The nonlinearity, originated from the interatomic interaction, is included in the equation through a mean-field term proportional to condensate density. Previously, several authors investigated the dynamics of GPE for a double-well potential in a two-mode approximation [3, 4, 5, 6, 7, 8, 9]. Novel features were found, e.g., the emergence of new nonlinear stationary states [5] and a variety of new crossing scenarios [9], nonzero adiabatic tunnelling probability [4, 7], etc, to name only a few. Among these findings, nonlinear Josephson oscillation and self-trapping phenomenon are of most interest. As well be known, for single particle in a symmetric double-well, the tunnelling dynamics is determined by the tunnelling splitting of two nearly degenerate eigenstates and tunnelling time or quantum oscillation period is inversely proportional to the energy splitting [10]. When atomic interaction emerges, the tunnelling between two-well is also observed, termed as nonlinear Josephson oscillation [3, 6, 8]. However, in this case, the oscillation period sensitively depends on the initial state but has little relation to the difference between the eigenenergies. More interestingly, with increasing the atomic interaction further (even it is repulsive), the Josephson oscillation between two wells is completely blocked, the BECs atoms in a symmetric double-well potential show a highly asymmetric distribution as if most atoms are trapped in one well [3]. This somehow counter-intuitive phenomenon is termed as self-trapping and has been observed in lab recently [11].

In the present paper, we extend to investigate tunnelling dynamics for BECs in a triple-well system [12, 13]

(schematically sketched as Fig.1), want to know how the nonlinear Josephson oscillation and self-trapping behave in this simplest multi-well system. This extension is not trivial because quantum tunnelling may happen between several wells simultaneously so that we expect that the tunnelling dynamics in the triple-well will show more interesting behavior. Moreover, the study of triple-well system will provide a bridge between the simple double-well and the multi-well, helping us understand the 'self-localized' phenomenon of BECs in the optical lattice [14].

Technically, to investigate the dynamics of triple-well system we resort to the Poincaré section method [15] that visualizes the motion of BECs in a reduced two dimensional phase plane. For our triple-well system, ignoring a total phase the dynamics is governed by a Hamiltonian with two freedoms. Its phase space is four-dimensional. However, the motions in a high-dimensional phase space (in our case, it is 4D) are difficult to trace. With us-

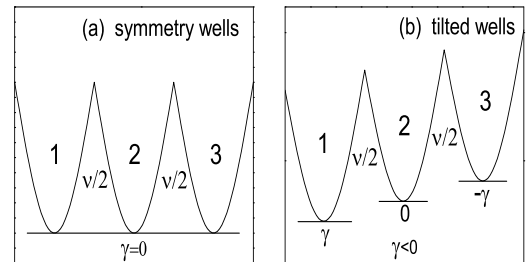


FIG. 1: The schematic sketch of our model. (a) The symmetric case ($\gamma = 0$); (b) The asymmetric case, ($\gamma < 0$; $\gamma > 0$) is the zero-point energy in each well respectively.

ing the Poicare section, we can investigate the motions of BEC in a reduced 2D phase plane.

Our paper is organized as follows. In Sec.II we introduce our model and show the unusual structure of the eigen-energies. In Sec.III we investigate nonlinear Josephson oscillations with using Poicare section method and demonstrate diverse types of the oscillations for BECs. In Sec.IV we investigate the transition from the Josephson oscillation to self-trapping of BECs in one-well as well as in two-well and show an irregular regime characterized by chaos. Our discussions are extended to tilted triple-well system in Sec.V. Final section is our discussions and conclusions.

II. MODEL

For the triple-well system and under mean field approximation, the wave function $\psi(r;t)$ of GPE is the superposition of three wave functions describing the condensate in each trap, i.e.,

$$\psi(r;t) = a_1(t)\psi_1(r) + a_2(t)\psi_2(r) + a_3(t)\psi_3(r); \quad (1)$$

Then the triple-well system is described by a dimensionless Schrodinger equation,

$$i\frac{d}{dt}\begin{pmatrix} a_1 \\ a_2 \\ a_3 \end{pmatrix} = \hat{H}\begin{pmatrix} a_1 \\ a_2 \\ a_3 \end{pmatrix}; \quad (2)$$

with the Hamiltonian

$$\hat{H} = \begin{pmatrix} 0 & 1 & 0 \\ c\frac{1}{2} & 0 & \frac{v}{2} \\ 0 & \frac{v}{2} & c\frac{1}{2} \end{pmatrix} \begin{pmatrix} a_1 \\ a_2 \\ a_3 \end{pmatrix} + \begin{pmatrix} 0 & 1 \\ \frac{v}{2} & 0 \end{pmatrix} \begin{pmatrix} a_1 \\ a_2 \end{pmatrix} + \begin{pmatrix} 0 & 1 \\ \frac{v}{2} & 0 \end{pmatrix} \begin{pmatrix} a_2 \\ a_3 \end{pmatrix}; \quad (3)$$

The total probability $|a_1|^2 + |a_2|^2 + |a_3|^2$ is conserved and is set to be unit. c is the mean field parameter denoting the atomic interaction and v is the coupling parameter, ϵ is the zero-point energy of the wells. The schematic sketch of the model is shown in Fig.1. In our following discussions, we focus on the case of repulsive interaction between atoms, i.e., $c > 0$.

With ignoring a total phase, the dynamics of the above three-level quantum system can be depicted by a classical Hamiltonian of two-degree freedom [12]. Let us set that, $n_1 = |a_1|^2; n_2 = |a_2|^2; n_3 = |a_3|^2; \phi_1 = \arg a_1 - \arg a_2; \phi_3 = \arg a_3 - \arg a_2$, use the constraint $n_1 + n_2 + n_3 = 1$, we can get the classical Josephson Hamiltonian,

$$H = \begin{pmatrix} n_1 & n_3 \end{pmatrix} + \frac{1}{2}c \begin{pmatrix} n_1^2 + n_3^2 + (1 - n_1 - n_3)^2 \end{pmatrix} + \frac{v}{2} \begin{pmatrix} 1 - n_1 - n_3 \end{pmatrix} \begin{pmatrix} \cos \phi_1 + \cos \phi_3 \end{pmatrix}; \quad (4)$$

and the corresponding canonical equations

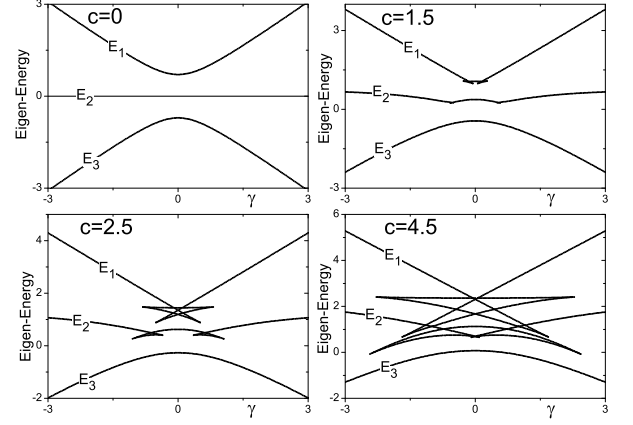


FIG. 2: The eigen-energy levels for different interaction strength. We have set $v = 1$.

$$\frac{dn_1}{dt} = -v \sin(\phi_1) \sqrt{n_1} \sqrt{1 - n_1 - n_3}; \quad (5a)$$

$$\frac{d\phi_1}{dt} = \frac{1}{2}c(2n_1 - 2(1 - n_1 - n_3)) + \frac{v \cos(\phi_1) \sqrt{1 - n_1 - n_3}}{2\sqrt{n_1}} + \frac{v \sqrt{n_1} \cos(\phi_1) + \cos(\phi_3) \sqrt{n_3}}{2\sqrt{1 - n_1 - n_3}}; \quad (5b)$$

$$\frac{dn_3}{dt} = -v \sin(\phi_3) \sqrt{n_3} \sqrt{1 - n_1 - n_3}; \quad (5c)$$

$$\frac{d\phi_3}{dt} = \frac{1}{2}c(2n_3 - 2(1 - n_1 - n_3)) + \frac{v \sqrt{n_1} \cos(\phi_1) + \cos(\phi_3) \sqrt{n_3}}{2\sqrt{1 - n_1 - n_3}} + \frac{v \cos(\phi_3) \sqrt{1 - n_1 - n_3}}{2\sqrt{n_3}}; \quad (5d)$$

The fixed point or minimum energy point of the classical Hamiltonian system (4) corresponds to the eigen-state of quantum system [7, 16]. To derive the analytical expressions of these fixed points is difficult, however, numerically, we can readily obtain them with exploiting the Mathematica Software [17]. We plot the eigenenergies as the function of the zero-point energy bias in Fig.2, they show unusual entangled star structure for the strong non-linearity.

For the weak interactions, the eigen-energy levels is very similar to linear case ($c = 0$). With increasing the nonlinearity (i.e., $c = 1.5$), topological structure of the upper level changes: two small loops emerge. When the interaction is stronger (i.e., $c = 2.5$), the two loops will collide and form a star structure, and then two more loops will emerge at the middle level E_2 . For still stronger interaction (i.e., $c = 4.5$), the star structure of the up-

per level entangles with the star structure in the lower level. However, we can still distinguish these levels because they have different relative phases. In fact, levels labeled by E_1 have relative phases ($\phi_1 = \pi$; $\phi_3 = 0$), levels labeled by E_2 have relative phases ($\phi_1 = 0$; $\phi_3 = 0$) or ($\phi_1 = 0$; $\phi_3 = \pi$), levels labeled by E_3 have relative phases ($\phi_1 = 0$; $\phi_3 = 0$).

The relation between the chemical potential and the above energy

$$E = \frac{c}{2} (\mu_1^4 + \mu_2^4 + \mu_3^4); \quad (6)$$

where μ_i denotes the chemical potential defined as $\hbar \mu_i$.

In the above calculations and henceforth, for convenience we set the coupling parameter as unit, i.e., $v = 1$.

III. THE SYMMETRIC TRIPLE-TRAP CASE, $\mu = 0$

Firstly we focus on the symmetric case, i.e., $\mu = 0$. The dependence of the energy levels on the interaction strength is exposed by Fig. 3. For the interaction strength is less than a critical value $c_1 = 1.56$, the level structure is similar to its linear counterpart except for some positive shifts on the energy values. For $c > c_1$, two more levels labeled as (E_{1a} ; E_{1b}) emerge. Actually, they correspond to the star structure of upper level E_1 in Fig. 2 and have relative phases of ($\phi_1 = \pi$; $\phi_3 = 0$). When the interaction strength is still stronger and exceeds the second critical value $c_2 = 4.06$, the other two more energy levels labeled as (E_{2a} ; E_{2b}) emerge. They correspond to the star structure of middle level E_2 in Fig. 2 and have the same relative phases as that of E_2 .

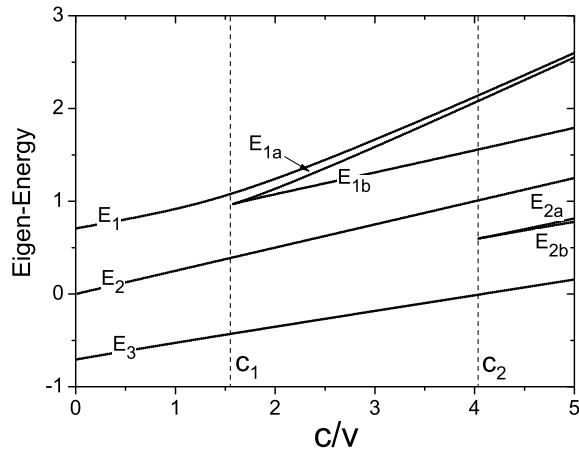


FIG. 3: When $\mu = 0$, the energy levels vary with the interaction strength c/v , where we set $v = 1$.

The stability of the corresponding eigen-states can be evaluated by the eigen-values of the Jacobian of the classical Josephson Hamiltonian (4).

$$J = \begin{pmatrix} \frac{\partial^2 H}{\partial n_1 \partial n_1} & \frac{\partial^2 H}{\partial n_1 \partial n_2} & \frac{\partial^2 H}{\partial n_1 \partial n_3} & \frac{\partial^2 H}{\partial n_1 \partial \phi_1} \\ \frac{\partial^2 H}{\partial n_2 \partial n_1} & \frac{\partial^2 H}{\partial n_2 \partial n_2} & \frac{\partial^2 H}{\partial n_2 \partial n_3} & \frac{\partial^2 H}{\partial n_2 \partial \phi_2} \\ \frac{\partial^2 H}{\partial n_3 \partial n_1} & \frac{\partial^2 H}{\partial n_3 \partial n_2} & \frac{\partial^2 H}{\partial n_3 \partial n_3} & \frac{\partial^2 H}{\partial n_3 \partial \phi_3} \\ \frac{\partial^2 H}{\partial \phi_1 \partial n_1} & \frac{\partial^2 H}{\partial \phi_1 \partial n_2} & \frac{\partial^2 H}{\partial \phi_1 \partial n_3} & \frac{\partial^2 H}{\partial \phi_1 \partial \phi_1} \end{pmatrix} : \quad (7)$$

The eigen-values of the above Jacobian have their correspondence of the Bogoliubov excitation spectrum of BECs. Pure imaginary values indicates to a stable BECs state, whereas emergence of real values implies the unstable for BECs and lead to a rapid production of the Bogoliubov quasi-particles [18]. From calculating the above Jacobian matrix and making diagonalization we know that, the states corresponding to level E_{1b} and level E_{2b} are unstable, others are stable.

A. Linear Josephson Oscillation Solution

For the linear Josephson oscillation, i.e., $c = 0$, the system is analytically solvable. The solutions of ($a_1; a_2; a_3$) are

$$a_1 = C_2 \cos\left(\frac{v}{2}t + C_3\right) + C_1; \quad (8a)$$

$$a_2 = C_4 \cos\left(\frac{v}{2}t + C_5\right); \quad (8b)$$

$$a_3 = \left(C_2 \cos\left(\frac{v}{2}t + \frac{T}{2}\right) + C_3\right) + C_1; \quad (8c)$$

Where C_i are parameter determined by initial conditions

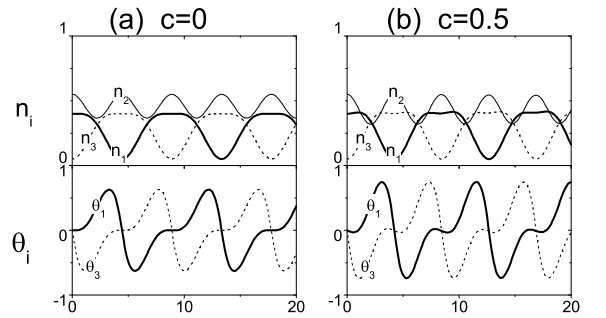


FIG. 4: The evolutions of n_1 (heavy line), n_2 (thin line), n_3 (dashed line) and ϕ_1 (heavy line), ϕ_2 (thin line), ϕ_3 (dashed line) in symmetric wells for linear case (a) and weak interactions case (b), with the same initial values ($n_1 = 0.4; n_3 = 0.05; \phi_1 = 0; \phi_3 = 0$).

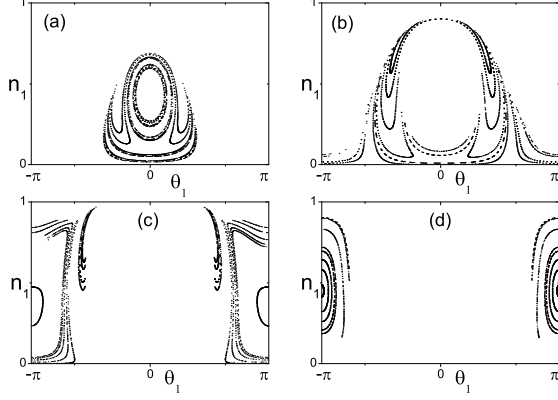


FIG. 5: The Poincaré section at $\theta_3 = 0$ for $c=v = 0.5$ with different energy E . (a) $E = 0.4$, (b) $E = 0.1$, (c) $E = 0.2$, (d) $E = 0.5$.

$$C_2 \cos C_3 + C_1 = a_1(0); \quad (9a)$$

$$C_4 \cos C_5 = a_2(0); \quad (9b)$$

$$C_2 \cos C_3 - C_1 = a_3(0); \quad (9c)$$

$$\frac{v}{2} C_2 \sin C_3 = i \frac{v}{2} a_2(0); \quad (9d)$$

$$\frac{v}{2} C_4 \sin C_5 = i \frac{v}{2} (a_1(0) + a_3(0)); \quad (9e)$$

and the constraint

$$j_1(0)^2 + j_2(0)^2 + j_3(0)^2 = 1; \quad (10)$$

From the above explicit expressions, we see that a_1, a_2 and a_3 vary with respect to time periodically. They share a common period that is inversely proportional to the coupling parameter, i.e., $T = 2\pi/2 = \pi/v$. Actually, the frequency is just the bias between eigen-energy levels. With initial conditions, the coefficients C_i will be fixed by using (9). In our case, $C_1 \neq 0$, so the period of population n_1 and n_3 is twice the period of n_2 , and compared with n_1 , variable n_3 has a phase delay of half-period. The above analysis is confirmed by our numerical simulations as shown in Fig. 4 (a).

B. Weak Interaction cases, $c < c_1$

The dynamics of this two-freedom system could be visualized from Poincaré section [15]. We do this by solving the canonical equations (5d) numerically and then plotting θ_1 and n_1 at each time that $\theta_2 = 0$ and $\dot{\theta}_2 < 0$. Notice the total energy is conserved, therefore the Poincaré sections consists of a picture panel where each picture corresponds a fixed energy.

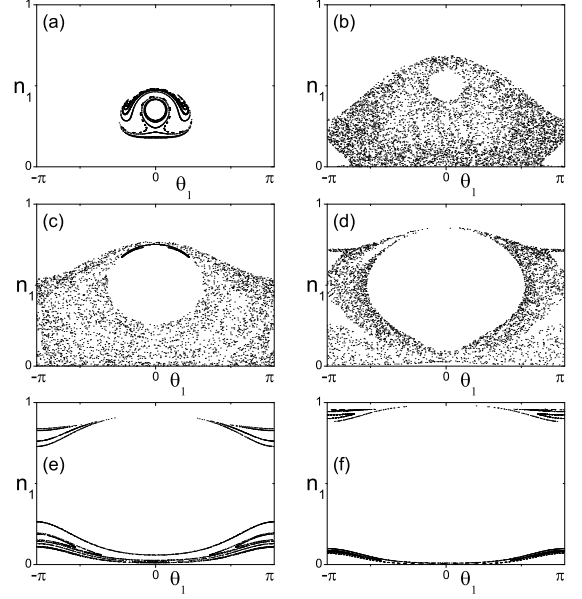


FIG. 6: The Poincaré section at $\theta_3 = 0$ for $c=v = 5$ with different energy E . (a) $E = 0.3$, (b) $E = 0.8$, (c) $E = 1.1$, (d) $E = 1.5$, (e) $E = 1.9$, (f) $E = 2.3$.

For the linear case, all of motions share a common period exactly, and the Poincaré section is some isolated points. With weak interactions, the periodicity will be destroyed, and the motions become periodic or quasi-periodic, corresponding Poincaré section is plotted in Fig. 5, where we see the section plane is full of stable islands. However, in this case the motion is similar to the linear case if they have the same initial values, as shown in Fig. 4 (a), 4 (b).

C. Strong Interaction Cases, $c > c_2$

When the interaction is strong, the nonlinear effect is dominant, accordingly the Poincaré section is complicated, as shown in Fig. 6, where we see many chaotic region except for some stable islands. In the islands, the motions are periodic or quasi-periodic whereas in the chaotic region the motions are irregular. In order to grasp the dynamical property in this situation, we have simulated the motions for every regular islands numerically, and find that except for the oscillations like the linear or weak interaction case, as shown in Fig. 7 (a), there are also four types of new oscillations, as shown in Fig. 7 (b)-(e), respectively.

Fig. 7 (a) shows that the oscillation in well one is almost the same as that of well three except a phase delay of half-period. In order to compare with the linear or weak interaction case, we take the same initial value as that of

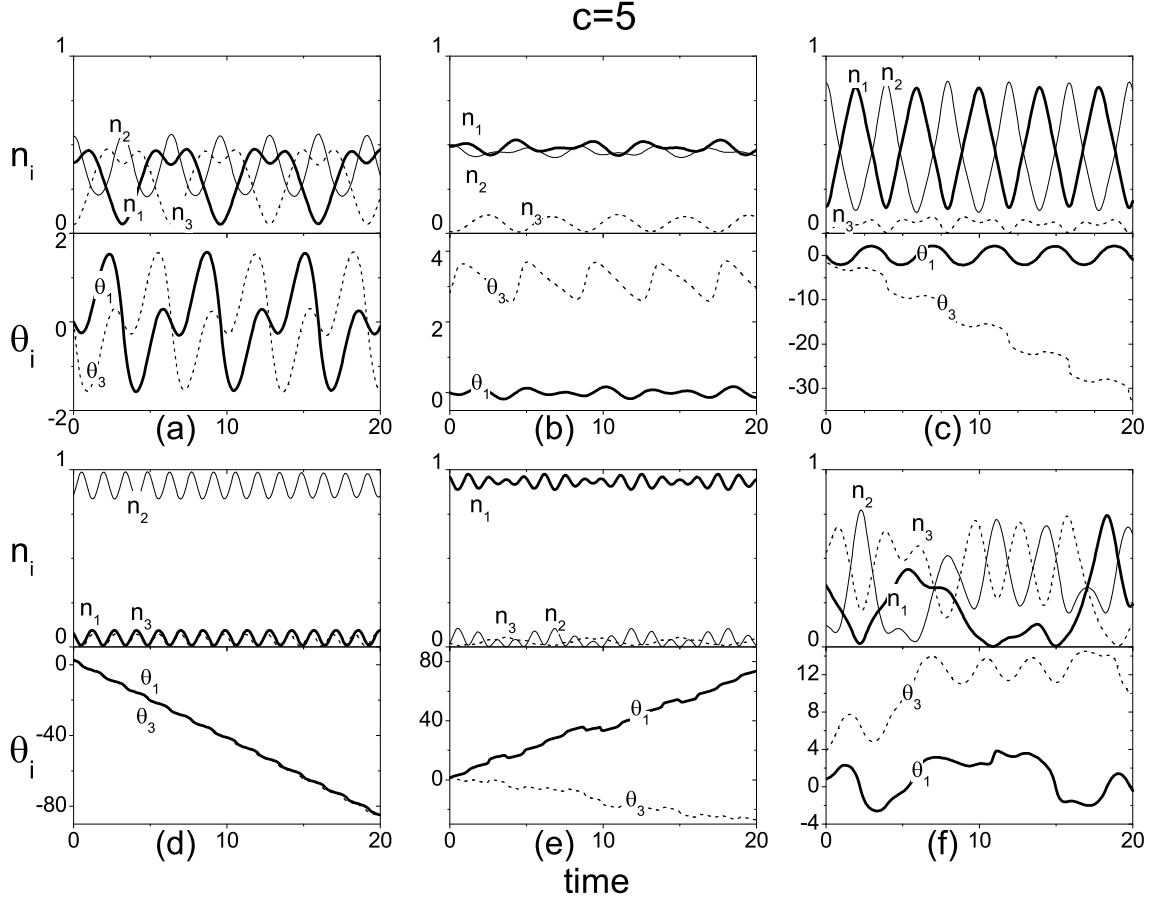


FIG. 7: The evolutions of n_1 (heavy line), n_2 (thin line), n_3 (dashed line) and θ_1 (heavy line), θ_3 (dashed line) in symmetric wells for strong interactions ($c=v=5$), with initial values (a) same to Fig. 4, ($n_1 = 0.4; n_3 = 0.05; \theta_1 = 0; \theta_3 = 0$); (b) ($n_1 = 0.49; n_3 = 0.012; \theta_1 = 0; \theta_3 = 2.82$); (c) ($n_1 = 0.15; n_3 = 0; \theta_1 = 0; \theta_3 = 0$); (d) ($n_1 = 0.076; n_3 = 0.066; \theta_1 = 2.54; \theta_3 = 2.79$); (e) ($n_1 = 0.96; n_3 = 0.02; \theta_1 = 1.36; \theta_3 = 1.34$); (f) ($n_1 = 0.348; n_3 = 0.532; \theta_1 = 0.817; \theta_3 = 3.843$).

Fig. 4. We see that their oscillations behavior is similar.

In addition to the case shown in Fig. 7 (a), the motions of BECs in triple-well can demonstrate very different behavior. Fig. 7 (b) shows that almost all of BECs atoms oscillate with small amplitude in two adjacent wells, i.e., well one and well two. The phase θ_1 oscillates around 0 and the phase θ_3 oscillates around π . The energy of these oscillations is closed to the eigen-energy of level labeled by E_{2a} , and the center they surrounded is near the fixed point corresponding to level E_{2a} . As mentioned before, this fixed point are stable point.

Fig. 7 (c) shows that almost all of BECs atoms oscillate with large amplitude in well one and well two, and the relative phase θ_1 is always oscillating around zero. These oscillations are regarded as oscillations in a reduced two-well trapped system. In fact, because n_3 is small and $c=v$

is very large, we can regard the term

$$H_1 = \sqrt{\frac{p_1}{1-n_1}} \sqrt{\frac{p_3}{1-n_3}} \cos(\theta_3) \quad (11)$$

as a perturbation. Using the generating function

$$G = v g(J_1; J_2) \sin(\theta_3) + J_1 \theta_1 + J_2 \theta_3: \quad (12)$$

Where

$$g(J_1; J_2) = \frac{\sqrt{\frac{p_1}{1-J_1}} \sqrt{\frac{p_3}{1-J_2}}}{c(1 - \frac{J_1}{2J_2})}:$$

Then the Hamiltonian becomes

$$H^0 = \frac{1}{2} c (2J_1^2 + 2J_2J_1 - 2J_1 + 2J_2^2 - 2J_2 + 1) + \sqrt{\frac{p_1}{1-J_1}} \sqrt{\frac{p_3}{1-J_2}} \cos(\theta_1): \quad (13)$$

The new canonical variables have relations with the old canonical variables

$$n_1 = J_1; \quad (14a)$$

$$n_3 = J_2 + v \cos(\phi) g(J_1; J_2); \quad (14b)$$

$$\phi = \phi_1 + v \sin(\phi) g^{(1;0)}(J_1; J_2); \quad (14c)$$

$$\phi_2 = \phi_2 + v \sin(\phi) g^{(0;1)}(J_1; J_2); \quad (14d)$$

Since the action variable J_2 is constant, the action-angle variables $J_1; \phi_1$ can be solved first from the new canonical equations (14). Notice that $J_1 = n_1$ is the population in well one, ϕ_1 is the relative phase of quantum state in well one and well two. The oscillations shown in Fig.7 (c) just like the zero-phase mode oscillations in a two-well trapped system.

Fig.7 (d) and 7 (e) show self-trapping of BECs in the middle well and self-trapping in one side well respectively. These motions have a close relations to the property of fixed points, and will be discussed in detail at the next section.

Fig.7 (f) shows the chaotic trajectory which corresponds to the chaotic region in the Poincare section. In this case, the population in each well shows irregular oscillation with respect to time.

IV. TRANSITION TO SELF-TRAPPING

A. Self-Trapping in One Well

Self-trapping is caused by the nonlinear interactions. For symmetric two-well system, as we have known, self-trapping happens only when the interaction parameter exceeds a critical value. By calculating the averaged population for same initial value $a_1(0) = 1; a_2(0) = 0$ with different interaction strength $c=v$, we show this in Fig.8 (a). The Hamiltonian used for calculation is $\hat{H} = \frac{c}{2} J_1^2 + \frac{v}{2} J_2^2$. It is clearly shown that, when $c=v > 2$ the averaged n_1 is no longer zero indicating the beginning of the self-trapping. Soon after that, with increasing the interaction the BECs will be trapped in well one completely. Because the transition corresponds to crossing over a separatrix from oscillation to liberation, at the transition point $c=v = 2$ the scaling law follows a logarithm function [19, 20].

For our triple-well system, the high-dimensional phase space permits the existence of chaos and the smooth movement of the fixed points to the boundary (the latter point will be clearly shown in Fig.9). So we expect that the transition to self-trapping in triple-well system will show distinguished property from that of double-well system. To demonstrate it, we calculate the time averaged population for different interactions with the initial conditions $n_2(0) = 1$ and $n_1(0) = 1$, denoting initial BECs

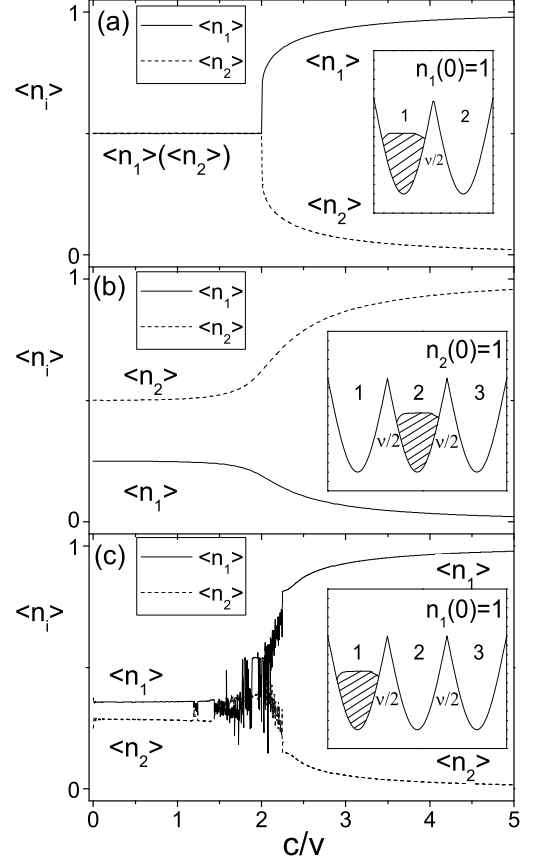


FIG. 8: The average of $n_1; n_2$ for different interactions $c=v$ in two-well system (a) and triple-well system (b,c), with initial value (a) $n_1(0) = 1$, (b) $n_2(0) = 1$, (c) $n_1(0) = 1$. The schematic sketch of the potential is shown in the figures.

uploaded in middle well and left-hand well, respectively. The results are shown in Fig.8 (b), 8 (c).

For the linear case, i.e., $c = 0$, in Fig.8 (b), substituting $(a_1 = 0; a_2 = 1; a_3 = 0)$ to (9), we can get one set of C_i

$$C_1 = 0; C_2 = \frac{1}{2}; C_3 = \frac{1}{2}; C_4 = 1; C_5 = 0;$$

Then from Eq.(8) we have the averaged populations

$$\langle n_1 \rangle = \langle n_3 \rangle = \frac{1}{2}; \langle n_2 \rangle = \frac{1}{2};$$

Likewise, in Fig.8 (c), substituting $(a_1 = 1; a_2 = 0; a_3 = 0)$ to (9), we can get one set of C_i

$$C_1 = \frac{1}{2}; C_2 = \frac{1}{2}; C_3 = 0; C_4 = \frac{1}{2}; C_5 = \frac{1}{2};$$

From Eq.(8) we have the averaged populations

$$\langle n_2 \rangle = \frac{1}{2}; \langle n_1 \rangle = \langle n_3 \rangle = \frac{1}{2};$$

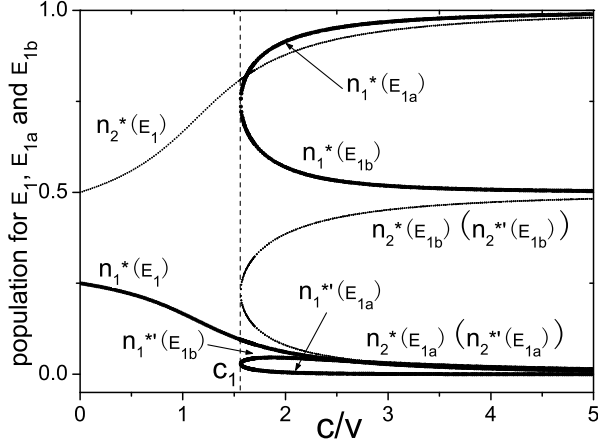


FIG. 9: The population n_1 (heavy line) and n_2 (thin line) for the levels labeled by E_1 , E_{1a} and E_{1b} in Fig.3.

For the weak interaction, i.e., $c < c_1$, the averaged populations are still similar to the linear case. However, when the interaction strength is close to the critical point c_1 , the averaged populations changed dramatically. For Fig.8 (b), the averaged population $\langle n_2 \rangle$ increases monotonically and smoothly to unit. No scaling law are observed. This is due to the fact that in the 4D phase space the fixed point can move smoothly to the boundary without through any bifurcation. For Fig.8 (c), the averaged populations become turbulence near the critical point, this is a result of chaotic trajectory in the phase space. Meanwhile, $\langle n_1 \rangle$ and $\langle n_3 \rangle$ are no longer equal. When the interaction is larger than 2.25, the averaged population $\langle n_1 \rangle$ becomes smooth and tends to unit rapidly.

For triple-well system, when the interaction strength exceeds the critical value c_1 , as mentioned before, new levels E_{1a} , E_{1b} will appear, accordingly new fixed points will emerge, and the phase space will tend to be divided into several subspace around the stable fixed points. In Fig.9 we plot populations n_1 and n_2 for the levels labeled by E_1 , E_{1a} and E_{1b} as a function of c/v . Corresponding to eigenenergy E_{1a} there are two eigen-states, denoted by n_1 and n_1^0 respectively. The same thing happens to level E_{1b} . Recall that E_1 , E_{1a} are stable levels. When the interaction is very strong, the averaged population $\langle n_2 \rangle$ of the motions of BECs uploaded initially in the middle well is close to $n_2(E_1)$, while $\langle n_1 \rangle$ of the motions of BECs uploaded initially in well one is close to $n_1(E_{1a})$, as shown in Fig.8 (b), Fig.8 (c).

B. Self-Trapping in Two Wells

In the above, we have investigated the self-trapping of BECs in single well. In this part, we will investigate

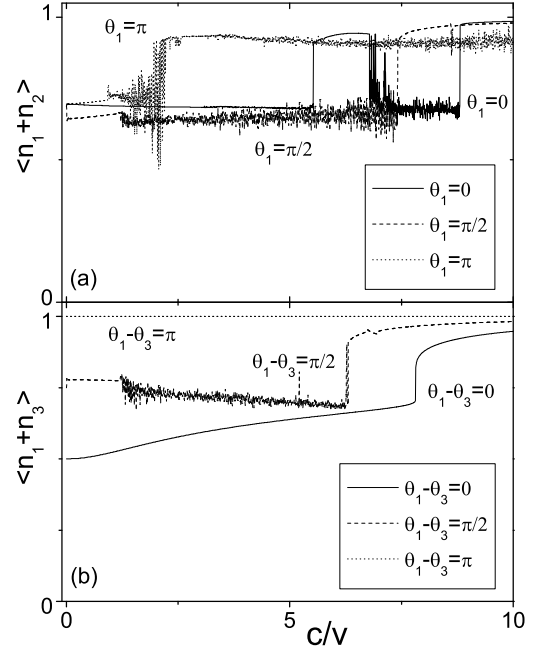


FIG. 10: The mean value of (a) $\langle n_1 + n_2 \rangle$ and (b) $\langle n_1 + n_3 \rangle$ with initial value (a) $(n_1 = 0.5; n_2 = 0.5; n_3 = 0)$, (b) $(n_1 = 0.5; n_2 = 0; n_3 = 0.5)$ for different relative phase.

whether the BECs atoms can be self-trapped only in two wells.

Considering the interference, the initial relative phase should be very important. So we calculate the mean value of $\langle n_1 + n_2 \rangle$ as a function of c/v for different phase θ_1 with initial value $(n_1 = 0.5; n_2 = 0.5; n_3 = 0)$, and the mean value of $\langle n_1 + n_3 \rangle$ as a function of c/v for different phase $\theta_1 - \theta_3$ with initial value $(n_1 = 0.5; n_2 = 0; n_3 = 0.5)$, respectively. The main results are shown in Fig.10.

It is shown that, with increasing the atomic interaction BECs will be trapped in the two wells where it is initially uploaded and the Josephson oscillation can be completely blocked. Both cases also suggest that the relative phase can dramatically influence the transition to self-trapping for BECs. In Fig.10 (a), when relative phase is zero, the Josephson oscillation and the self-trapping can emerge alternately. Whereas, for case of Fig.10 (b), value of the relative phase gives a robust self-trapped BECs. In both cases, we also see the occurrence of the chaos making the curves look irregular. Interestingly, the onset of chaos can also be controlled by the relative phase, e.g., the vanishment of the relative phase will reduce the chaos and make the BECs safely turn from oscillation state to self-trapping state as shown in Fig.10 (b).

V. TILTED TRIPLE-WELL, $\epsilon = 0$

In this section we extend the above discussions to the tilted triple-well system. In this system, the diverse type of Josephson oscillations also emerge around the eigenstates. In light of the energy spectra Fig.2, we can readily find out the parameter regime for different kinds of oscillations. So, we will focus on the transition to self-trapping that is of more interest. We want to see how the transition is influenced by tilting the wells.

A. Linear Oscillation Solutions

For the linear case, i.e., $c = 0$, the system is analytically solvable. So the solutions of $(a_1; a_2; a_3)$ are

$$a_1 = \frac{1}{2}C_4 \cos\left(\frac{v^2}{2} + \frac{1}{2}t + C_5\right) + \frac{1}{2\left(\frac{v^2}{2} + \frac{1}{2}\right)} \left(C_2 \cos\left(\frac{v^2}{2} + \frac{1}{2}t + C_3\right) + vC_1 \right); \quad (15a)$$

$$a_2 = \frac{1}{\frac{v^2}{2} + \frac{1}{2}} \left(\frac{v}{2}C_2 \cos\left(\frac{v^2}{2} + \frac{1}{2}t + C_3\right) + C_1 \right); \quad (15b)$$

$$a_3 = \frac{1}{2}C_4 \cos\left(\frac{v^2}{2} + \frac{1}{2}t + C_5\right) - \frac{1}{2\left(\frac{v^2}{2} + \frac{1}{2}\right)} \left(C_2 \cos\left(\frac{v^2}{2} + \frac{1}{2}t + C_3\right) + vC_1 \right); \quad (15c)$$

Where C_i are complex integral constant and like the symmetric case, determined by initial conditions.

It is clear that $a_1; a_2$ and a_3 vary with respect to time periodically. The period $T = 2\pi = \frac{2\pi}{\frac{v^2}{2} + \frac{1}{2}}$.

B. Transition to Self-Trapping

When the interaction is strong we still observe the self-trapping of BECs in the tilted system. We plot the averaged populations in their dependence of the interaction strength with choosing parameter $\epsilon = 1$ and initial conditions $n_1 = 1, n_2 = 1$ and $n_3 = 1$ in Fig.11 (a), 11 (b) and 11 (c) respectively. The schematic sketch of the wells is shown in Fig.1 (b).

For Fig.11 (a), when $c/v = 0$, with the initial conditions $(a_1 = 1; a_2 = 0; a_3 = 0)$, we derive one set of C_i

$$C_1 = v/2; C_2 = iv/2; C_3 = \arccos\left(\frac{v}{2}\right);$$

$$C_4 = \frac{v}{v^2 + 2}; C_5 = \arccos\left(\frac{v}{v^2 + 2}\right);$$

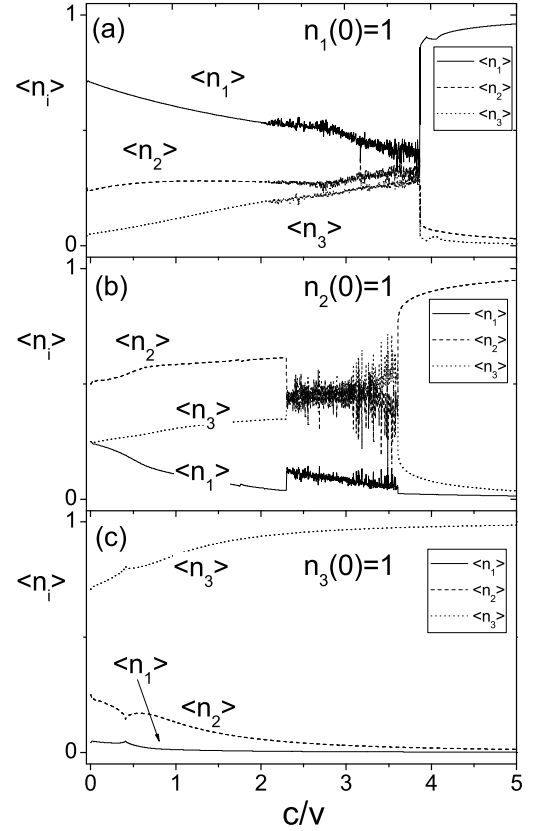


FIG. 11: The average of n_i for different interactions c/v in asymmetric wells $\epsilon = 1$ with initial value (a) $n_1(0) = 1$, (b) $n_2(0) = 1$, (c) $n_3(0) = 1$.

By integrating $\dot{a}_i(t)^2$ with respect to time and making average over time we obtain the averaged population analytically from (15),

$$\langle n_1 \rangle = 1/4; \langle n_2 \rangle = 1/4; \langle n_3 \rangle = 1/4;$$

With increasing the nonlinearity, the averaged population in well one $\langle n_1 \rangle$ decrease at first, and then become turbulence, indicating chaotic motions. When the interaction parameter is larger than 3.9, the averaged population jumps up and tends to unit soon after.

In Fig.11 (b), initial condition is $(a_1 = 0; a_2 = 1; a_3 = 0)$. Similarly the averaged populations are readily obtained for the linear case, $\langle n_1 \rangle = 1/4; \langle n_2 \rangle = 1/2; \langle n_3 \rangle = 1/4$. With increasing the nonlinearity, the averaged population $\langle n_2 \rangle$ increases smoothly at beginning, passes a turbulence interval [2.3; 3.6], and then jumps up and tends to unit. Another interesting phenomenon in the process is that the averaged population in well three is always larger than that of well one in the presence of the nonlinearity, even though in this case the zero-point energy

of well three is obviously greater than that of well one. This somehow counterintuitive phenomenon is clearly the consequence of the nonlinearity.

In Fig.11(c), when $c=v=0$, with the initial conditions ($a_1=0; a_2=0; a_3=1$), the averaged populations have some correspondence to that of Fig.11(a) due to behind symmetry, i.e., $\langle n_{1i} \rangle = 1/24; \langle n_{2i} \rangle = 1/4; \langle n_{3i} \rangle = 17/24$: With increasing the nonlinearity, the averaged population in well three $\langle n_{3i} \rangle$ increases monotonically and smoothly to unit.

With comparing Fig.11 to Fig.8, we find that, the smooth transition of the BECs in middle well to self-trapping in the symmetric triple-well is broken by tilting the wells, and lifting the well three makes BECs smoothly transit to self-trapping states without losing their stability. Fig.11 also shows that, BECs in higher wells are easily self-trapped. From the above discussions, we conclude that the transition to self-trapping of BECs in triple-well systems can be effectively controlled by tilting the wells.

VI. CONCLUSIONS

We have presented a comprehensive analysis of the tunnelling dynamics for BECs in a triple-well trap both numerically and analytically. Diverse energy levels are demonstrated. Behind these unusual level structures, we reveal many new types of nonlinear Josephson oscillation.

We also study the self-trapping of BECs in one-well as well as in the two-well and investigate the transition from nonlinear Josephson oscillation to self-trappings. Distinguished from the double-well case, no scaling law is observed at the transition and the transition may be accompanied by an irregular regime where the motions are dominated by chaos. We also find that the transition can be effectively controlled by the relative phase between wells and tilting the wells. In the present experiments, the double-well is realized in the optical traps with using a blue-detuned light to form a barrier. With the same technique, the triple-well is also possibly realized in the optical traps. We hope our theoretical discussion will stimulate the experiments in the direction.

Acknowledgement

This work was supported by National Natural Science Foundation of China (No.10474008,10604009), Science and Technology fund of CAEP, the National Fundamental Research Programme of China under Grant No. 2005CB3724503, the National High Technology Research and Development Programme of China (863 Programme) international cooperation program under Grant No.2004AA121220, and Hebei Natural Science Foundation Project under Grant No.: A2006000128.

[*] Liu_Jie@iapcm.ac.cn

- [1] M. H. Anderson, M. R. Matthews, C. E. Wieman, and E. A. Cornell, Science 269, 198 (1995); K. B. Davis, M. O. Mewes, M. R. Andrews, N. J. van Druten, D. S. Durfee, D. M. Kurn, and W. Ketterle, Phys. Rev. Lett. 75, 3969 (1995); C. C. Bradley, C. A. Sackett, J. J. Tollett and R. G. Hulet, ibid. 75, 1687 (1995).
- [2] L. Pitaevskii and S. Stringari, Bose-Einstein Condensation (Oxford University Press, Oxford, 2003).
- [3] A. Smerzi, S. Fantoni, S. Giovanazzi, and S. R. Shenoy, Phys. Rev. Lett. 79, 4950 (1997); G. J. M. Albus, J. Cn-mey, E. M. Wright, and D. F. Walls, Phys. Rev. A 55, 4318 (1997).
- [4] Biao Wu and Qian Niu, Phys. Rev. A 61, 023402 (2000); O. Zobay and B. M. Garraway, Phys. Rev. A 61, 033603 (2000); R. D'Agosta and C. Presilla, Phys. Rev. A 65, 043609 (2002).
- [5] M. Holthaus, Phys. Rev. A 64, 011601(R) (2001).
- [6] S. Raghavan, A. Smerzi, S. Fantoni, and S. R. Shenoy, Phys. Rev. A 59, 620 (1999).
- [7] Jie Liu, Libin Fu, Bi-Yao Ou, Shi-Gang Chen, Dae-II Choi, Biao Wu, and Qian Niu, Phys. Rev. A 66, 023404 (2002).
- [8] Anthony J. Leggett, Rev. Mod. Phys. 73, 307 (2001), and references therein.
- [9] D. Witthaut, E. M. Graefe, and H. J. Korsch, Phys. Rev. A 73, 063609 (2006); Biao Wu and Jie Liu, Phys. Rev. Lett. 96, 020405 (2006).
- [10] L. D. Landau and E. M. Lifshitz, Quantum Mechanics (Pergamon Press, New York, 1997).
- [11] Michael A. Bieze, R. Gati, Jonas Fölling, S. Hunsmann, M. Cristiani, and M. K. Oberthaler, Phys. Rev. Lett. 95, 010402 (2005).
- [12] E. M. Graefe, H. J. Korsch, and D. Witthaut, Phys. Rev. A 73, 013617 (2006).
- [13] S. Mosemann and C. Jung, Phys. Rev. A 74, 033601 (2006).
- [14] The "self-trapping" of BECs in optical lattice has been observed experimentally, however the behind physics is not fully understood, refer to, T. Anker, M. A. Bieze, R. Gati, S. Hunsmann, B. Eiermann, A. Trombettoni, and M. K. Oberthaler, Phys. Rev. Lett. 94, 020403 (2005); Tristram J. Alexander, Elena A. Ostrovskaya, and Yuri S. Kivshar, Phys. Rev. Lett. 96, 040401 (2006); Roberto Livi, Roberto Franzosi, and Gian-Luca Oppo, Phys. Rev. Lett. 97, 060401 (2006); Bingbing Wang, Panming Fu, Jie Liu, and Biao Wu, e-print cond-mat/0601249 (2006).
- [15] A. J. Lichtenberg, and M. A. Leiberman, Regular and Stochastic Motion (Springer-Verlag, New York, 1983); L. E. Reichl, The Transition to Chaos (Springer-Verlag, New York, 1992).
- [16] Jie Liu, Biao Wu, and Qian Niu, Phys. Rev. Lett. 90, 170404 (2003).
- [17] An introduction of Mathematica could be found from <http://www.wolfram.com/>.
- [18] Jie Liu, Chuanwei Zhang, Mark G. Raizen, and Qian Niu, Phys. Rev. A 73, 013601 (2006); Chuanwei Zhang, Jie Liu, Mark G. Raizen, and Qian Niu, Phys. Rev. Lett.

92, 054101 (2004).
 [19] Guan-Fang Wang, Li-Bin Fu, and Jie Liu, Phys. Rev. A
 73, 013619 (2006).

[20] Li-Bin Fu and Jie Liu, eprint cond-mat/0609337 (2006).